Supporting Information

Jackson et al. 10.1073/pnas.1312006110

SI Discussion

A few of our histological observations warrant additional discussion.

Silver staining is sometimes used in studies of neurodegenerative diseases involving protein misfolding as a method to label pathological protein deposits. However, it has also been widely used in other types of neurodegeneration, such as that caused by stroke or by mechanically cutting specific areas. H&E stains are widely used for all types of tissue, but their usefulness for the observation of dead or dying cells is limited to a very short period, as most cellular debris is quickly removed. The ideal situation would be for remnants of dead neurons to remain detectable long after their demise. The disintegrative-degeneration silver staining method helps to expand the window of time for which cellular remnants are still detectable (1). By applying this approach, we found that the fatal familial insomnia (FFI) mice, already known to undergo thalamic neuronal loss, had strong silver staining there, as expected. Although we saw neuropathologic processes in the CA1 region of the hippocampus of Creutzfeldt–Jakob disease (CJD) mice, we wanted to determine if there was cellular debris in this region or in regions anatomically connected to it (in addition to CA3, other regions of the brain signal into CA1, including specific regions of the thalamus). Unfortunately, the silver stain experiments did not reveal any obvious areas of cell debris in the CJD mice. As this brain-wide approach had negative results, experiments to more precisely identify which neurons are causing the neuropathologic conditions will need to focus on more specific regions (such as CA3 or the thalamus) or to use tract-tracing tools.

The observation of CJD aggregates by light microscopy but not EM, and the exact opposite observation for FFI aggregates, was perplexing, as are many aspects of prion biology. Nearly 100 deposits in FFI brains were imaged, and many more were observed. They typically were perinuclear and near lipofuscin deposits, lipid-rich pathological degradation products often seen in other neurodegenerative diseases, including Alzheimer's and Parkinson diseases. Immunolabeling of prion protein (PrP) is notoriously difficult, as indicated by the many reports citing contradictory interpretations of the localization of WT PrP (2–7). This is mainly because of PrP requiring extensive fixation, which severely weakens antigenicity. The extensive fixation is required to immobilize PrP because it normally resides in a fluid lipid environment (4). We also had difficulties labeling PrP in our standard EM preparations, but observed some specific staining in the deposits when using milder fixation. The inability to observe aggregates in the CJD mice by EM was very surprising. We can only surmise that the deposits stain differently than those in FFI brains and were not discernible in the context of the surrounding tissue. The deposits are quite different in the different disease models, as the CJD deposits were typically in synapse-rich regions, distal to cell bodies, whereas the FFI aggregates were always intracellular, usually, if not exclusively, adjacent to neuronal nuclei.

Immunodetection of proteins involved in cell death pathways provides another approach and is sometimes used to verify the presence of a pathological state. Investigating proteins involved in cell-cycle activation has recently been used. We applied both methods in our experiments and found that some regions showed activation of cell death pathways whereas others instead showed activation of cell cycle pathways. A surprising outcome of these tests was the observation of abnormal staining of the CJD thalamus with cell death proteins, as this region appeared normal by all other tests. The finding of cell death proteins in a perinuclear location suggests the pathway had been activated but subsequently stalled. The CJD brains were also positive for the cell cycle proteins proliferating cell nuclear antigen (PCNA) and H2A.X, but in this case in the superior colliculus and striatum, respectively. It is likely that this reactivation of the cell cycle is also stalled. An enticing interpretation is that these two broadly opposed pathways are in competition, and future experiments should resolve this possibility. We conclude that the same toxic protein can cause different brain regions to react with unique responses.

SI Methods

Genome Manipulation. Procedures for generation of targeting constructs, mouse ES cell manipulation, and genotyping protocols were described previously (8). The CJD mutation was introduced into pWJPrP1 by using a pair of DNA oligomers, one with the sequence 5′-GGGGGAGAACTTCACGAAGACCG-ATGTGAAGATGATG and the other its reverse complement. 129/Ola ES cells were genetically modified and used to generate chimeric mice that were bred to C57BL/6N mice. These F1 offspring were bred to C57BL/6N mice, and their heterozygous offspring were then intercrossed to generate homozygous mice with a genetic background ~25% 129/Ola, 75% C57BL/6N, the same as for the WT and FFI mice. While mice with this mixed genetic background were being characterized, a subset was backcrossed for 12 generations, resulting in a theoretical background ~99.98% C57BL/6N. These backcrossed mice developed spongiosis and proteinase K (PK)-resistant PrP (PrP^{res}) deposits at the same age and high frequency as in the mixed-background mice.

Antibodies. Antibodies were purchased from BD Biosciences (adhesion molecule on glia or AMOG), Cayman Chemical (scrapie associated fibril32 or SAF32, SAF84), Cell Signaling (PCNA), Chemicon (apoptosis inducing factor, endonuclease G, GFAP), Covance (3F4), and Millipore (H2A.X). Cell cycle-related antibodies that were tested but showed no staining or no difference in staining (CDK4, cyclin D2, cyclin D3, mouse double minute 2 or MDM2, p21) were all from Santa Cruz. These negative results carry the caveat that there were often not positive controls in place.

Western blots were performed by using the chemiluminescent-based procedures described previously (8).

Immunohistochemistry was performed on formalin-fixed, paraffin-embedded 4-μm-thick sections as done previously (8). Grading of reactive gliosis followed guidelines described previously (9). PrP^{res} experiments for mutant brains and brains from mice infected with mutant brains were performed on paraffin-embedded brain sections cut at 4 μm. Slides were cleared in xylenes, treated with 98% (wt/vol) formic acid for 3 min, washed three times in PBS solution, slowly boiled via microwave oven in 10 mM citrate buffer, pH 6.0, allowed to cool to room temperature, and digested with 0.005 mg/mL PK (0.02 mg/mL for Tga20) for 30 min at room temperature, followed by PK inactivation with PBS solution washes and PMSF. An ABC kit from Vector Labs was then followed in combination with the SAF32, SAF84, or 3F4 PrP antibodies.

Clinical Measures of Disease. Automated mouse behavioral analysis (AMBA) experiments of CJD mice were run in parallel with the previously reported FFI mice, and used the same cohort of control mice. To simplify cross-comparisons, data presented here are in the same format, and the bin charts for 16-mo-old mice

were presented as they were in the previous report (8). A full description of AMBA methods and controls has been reported (10). The metric "awaken" measures any activity immediately following sleep and would be expected to be of longer duration for mice that are slow to transition to a second activity. "Urinate" is not scored accurately and was inactivated during the analysis but retained in the present table to maintain the same format as presented previously (8).

A cohort of mice not included for AMBA experiments was used for rotarod and burrow experiments. In our experience, mice older than 1 y perform poorly on the rotarod (i.e., remain on for short time periods) during their first attempts, independent of strain or health status. However, after a few training sessions, healthy mice will perform better. Therefore, mice were tested on three separate trials separated by 2 to 3 h for three consecutive days. Burrowing experiments were performed similar to previous descriptions (11) with a few changes. Pipes made of polyvinyl chloride were used as burrowing tubes. They were 20 cm in length with an inner diameter of 7.7 cm. The distance between the cage bottom and the lowest, inside surface of the tube was ~3.7 cm. Each tube was loaded with 800 mL of wood chip bedding, then placed in large cages. Mice were placed into these cages 1 h before the beginning of the dark cycle and were left overnight. The numbers of animals used for rotarod testing were as follows: WT, $n = 14$; CJD, $n = 11$; and FFI, $n = 19$. Numbers for burrow experiments were: WT, $n = 14$; CJD, $n = 9$; and FFI, $n = 9$.

MRI was performed following the procedure for the 9.4-T data in a previous work (12). The acquisition of high-resolution data, and thus smaller voxel sizes, resulted in weaker signals compared with our previous data with the FFI mice at 4.7 T.

Silver staining was performed by using the FD NeuroSilver Kit II from FD NeuroTechnologies.

Transmission Experiments. Mice were injected with CJD homogenates as done previously (8) and were examined weekly for signs of neurological disease by someone experienced with scoring neurological disease in mouse models of prion disease but blinded to the purpose of the experiment and to the genotypes and the number of mice predicted to stay healthy or become ill. WT mice lacking the 3F4 epitope were resistant to FFI inocula, most likely because of the 3F4 transmission barrier (8). Therefore, they were not challenged with CJD homogenates.

EM. For routine morphology, after profusion and excising, the tissue was further fixed in 2.5% glutaraldehyde, 3% paraformaldehyde with 5% sucrose in 0.1 M sodium cacodylate buffer (pH 7.4), and postfixed in 1% osmium in veronal-acetate buffer. The tissue was stained en bloc overnight with 0.5% uranyl acetate in veronal-acetate buffer (pH 6.0), then dehydrated and embedded in Spurr resin. Blocks were sectioned with a Leica ultracut UCT ultramicrotome with a DiATOME knife. Sections were stained with 2% uranyl acetate, and lead citrate. Sections were examined by using a FEI Tecnai Spirit at 80 kV and photographed with an AMT CCD camera. For immuno-EM, brains were fixed by perfusion with 2% paraformaldehyde in phosphate buffer, followed by fixation in paraformaldehyde/lysine/periodate fixative agent for 6 h. Tissue was infiltrated with cryoprotectant for 1 h with a mixture of 2.3 M sucrose in 0.1 M phosphate buffer containing 20% polyvinyl pyrrolidone, mounted on an aluminum nail, and quickly frozen in liquid nitrogen. Frozen sections (80 nm) were cut at −120° with an Leica Ultracut with FCS stage. Sections were labeled overnight in SAF32 PrP antibody diluted 1:5 followed by (5 nm) gold secondary antibody for 1 h. Grids were stained with 2% uranyl acetate for 20 min and absorption stained with 0.2% uranyl acetate (10 min) in 0.2% methylcellulose and 3.3% polyvinyl alcohol.

1. Switzer RC, 3rd (2000) Application of silver degeneration stains for neurotoxicity testing. *Toxicol Pathol* 28(1):70–83.
2. Bailly Y, et al. (2004) Prion protein (PrPc) immunocytochemistry and expression of the green fluorescent protein reporter gene under control of the bovine PrP gene promoter in the mouse brain. *J Comp Neurol* 473(2):244–269.
3. Barmada S, Piccardo P, Yamaguchi K, Ghetti B, Harris DA (2004) GFP-tagged prion protein is correctly localized and functionally active in the brains of transgenic mice. *Neurobiol Dis* 16(3):527–537.
4. Ford MJ, et al. (2002) A marked disparity between the expression of prion protein and its message by neurones of the CNS. *Neuroscience* 111(3):533–551.
5. Lainé J, Marc ME, Sy MS, Axelrad H (2001) Cellular and subcellular morphological localization of normal prion protein in rodent cerebellum. *Eur J Neurosci* 14(1):47–56.
6. Le Pichon CE, Firestein S (2008) Expression and localization of the prion protein PrP(C) in the olfactory system of the mouse. *J Comp Neurol* 508(3):487–499.
7. Mironov A, Jr., et al. (2003) Cytosolic prion protein in neurons. *J Neurosci* 23(18): 7183–7193.
8. Jackson WS, et al. (2009) Spontaneous generation of prion infectivity in fatal familial insomnia knockin mice. *Neuron* 63(4):438–450.
9. Sofroniew MV, Vinters HV (2010) Astrocytes: biology and pathology. *Acta Neuropathol* 119(1):7–35.
10. Steele AD, Jackson WS, King OD, Lindquist S (2007) The power of automated high-resolution behavior analysis revealed by its application to mouse models of Huntington's and prion diseases. *Proc Natl Acad Sci USA* 104(6):1983–1988.
11. Deacon RM (2006) Burrowing in rodents: A sensitive method for detecting behavioral dysfunction. *Nat Protoc* 1(1):118–121.
12. Faas H, et al. (2010) Context-dependent perturbation of neural systems in transgenic mice expressing a cytosolic prion protein. *Neuroimage* 49(3):2607–2617.

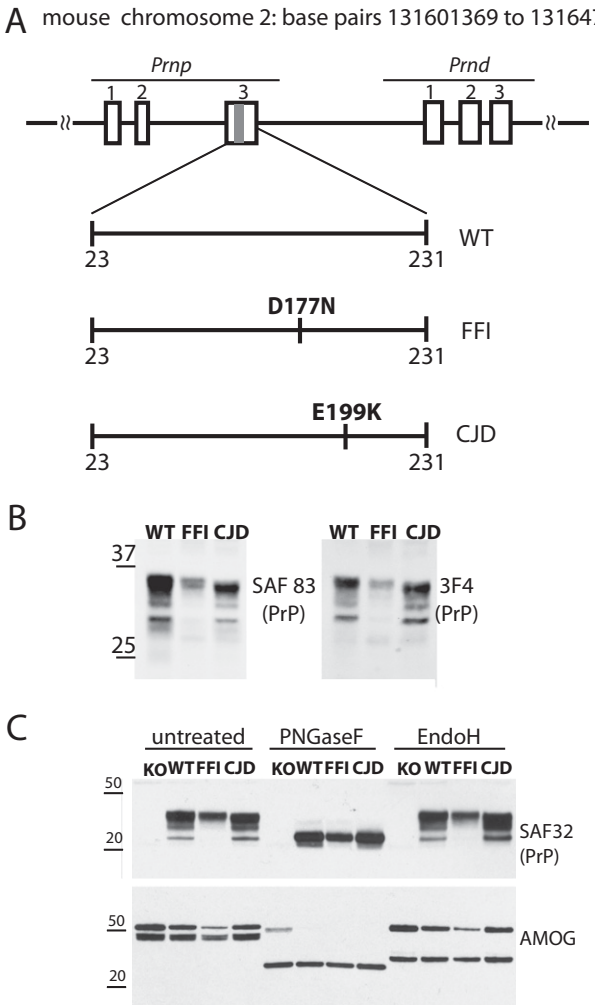

Fig. S1. (*A*) Schematic of PrP sequence differences expressed by different mouse lines. The top line depicts the *Prnp* genomic locus and the closely linked *Prnd* gene. All changes are made to the protein coding sequence in exon 3 of *Prnp* (grayed area). Underneath are horizontal lines depicting three forms of mature PrP expressed in the knock-in mice, which include amino acids 23 to 231 of a 254-aa protein, as, shortly after synthesis, signal sequences are clipped off. Positions of amino acid changes are indicated above vertical ticks on the horizontal lines. (*B*) Western analysis of 6-mo-old whole brain homogenates using SAF83 (*Left*) or 3F4 (*Right*) reveals steady-state levels of PrP are drastically reduced in FFI brains but only slightly reduced in CJD brains compared with controls. Differences in band intensity and migration rates indicate that glycosylation patterns were also different. Horizontal marks (*Left*) indicate molecular weight standards in kilodaltons. (*C*) Biochemical analysis of PrP trafficking through the secretory system indicates mutant PrPs are not grossly retained in the ER. Samples from 18-mo-old KO and knock-in mice (labeled as in *B*) were incubated at 37 °C for 1 h with no enzyme (untreated), PNGaseF, or endoglycosidase H (EndoH), and used to generate two Western blots in parallel: (*Upper*) used to detect PrP (SAF32) and (*Lower*) an unrelated glycoprotein for confirmation of enzymatic activity (AMOG).

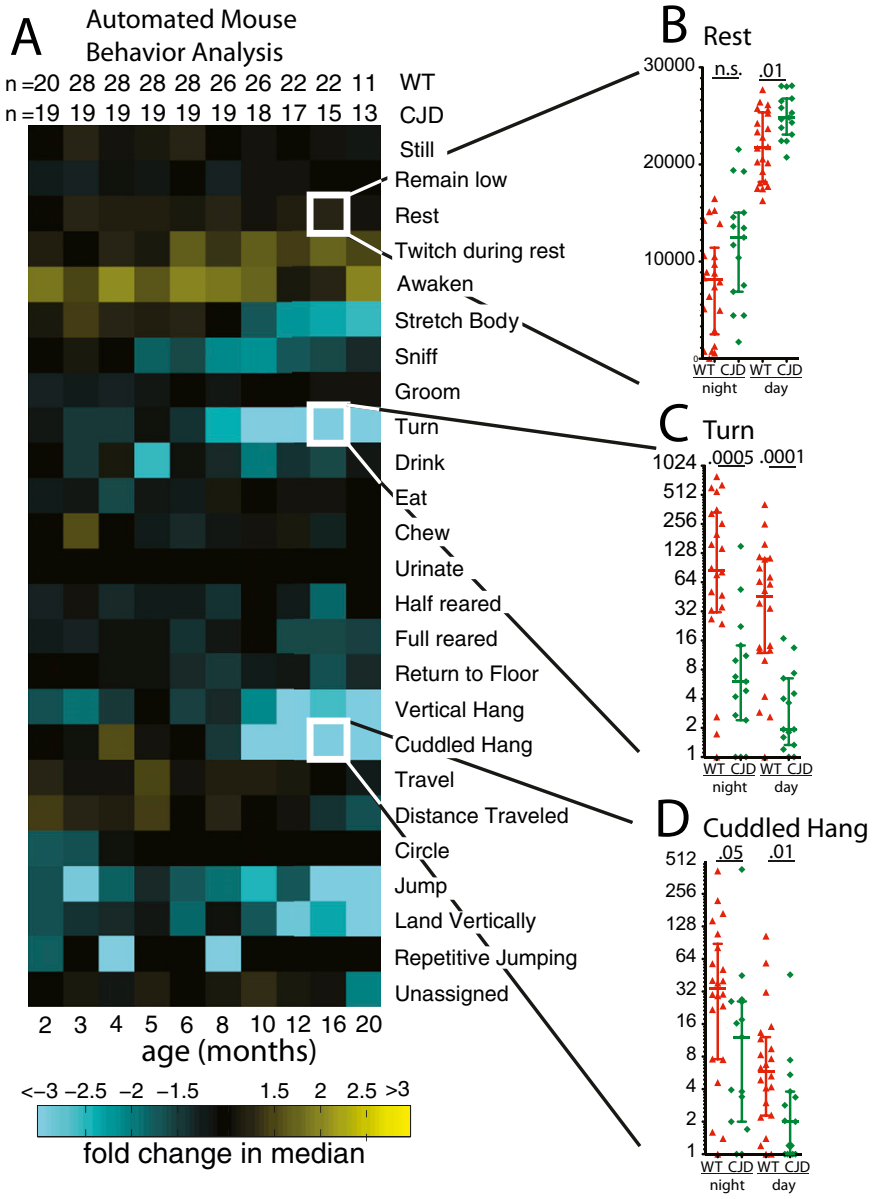

Fig. S2. (*A*) Phenotypic array representing median differences between WT and CJD mice for specific behaviors (*Right*). Yellow tiles depict comparisons for which the CJD mice performed the specific activity more than WT, and cyan tiles represent comparisons for which the CJD mice performed the specific activity less than WT mice. The brightness corresponds to the magnitude of the difference in median. The age in months is directly below the array. The number of animals for each comparison is immediately above the array, where the upper row indicates the number of WT mice and the lower row indicates the number of CJD mice. This is a copy of the array from Fig. 1 reproduced here to improve visualization in the context of *B*–*D*. (*B*–*D*) Scatter-plots of data collected during the first 10 h of night and the first 10 h of the following day. Numbers in the charts represent *P* value cutoffs.

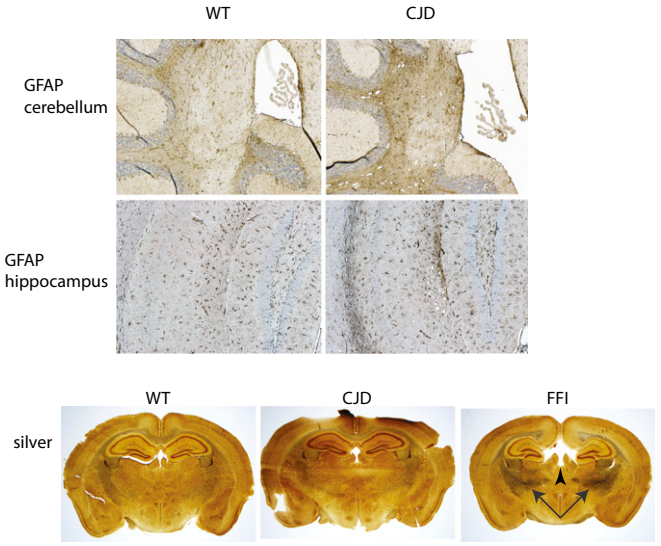

Fig. S3. Reactive gliosis in the cerebellum (*Top*) and hippocampus (*Middle*) of a CJD mouse brain (*Right*) revealed by IHC for GFAP. Silver staining of 30-μm-thick sections from WT, CJD, and FFI brains reveals neurodegenerated cells (arrows) and dilated ventricles (arrowhead) in FFI but not CJD brains.

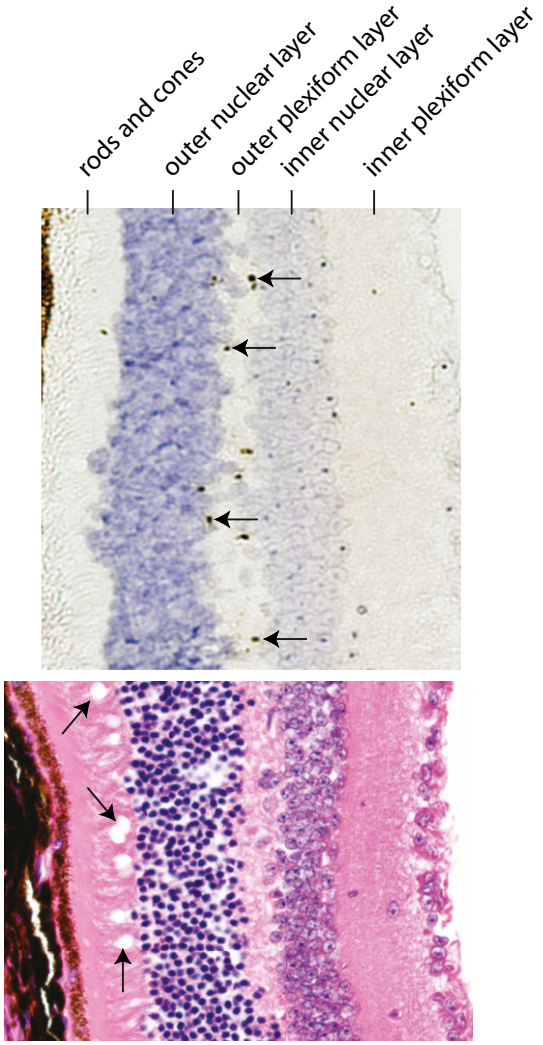

Fig. S4. In the retina, PrP aggregates are present in the outer plexiform layer (*Upper*, arrows), containing the neuropil of the rods and cones, which appear to be degenerating in the H&E stain (*Lower*, arrows).

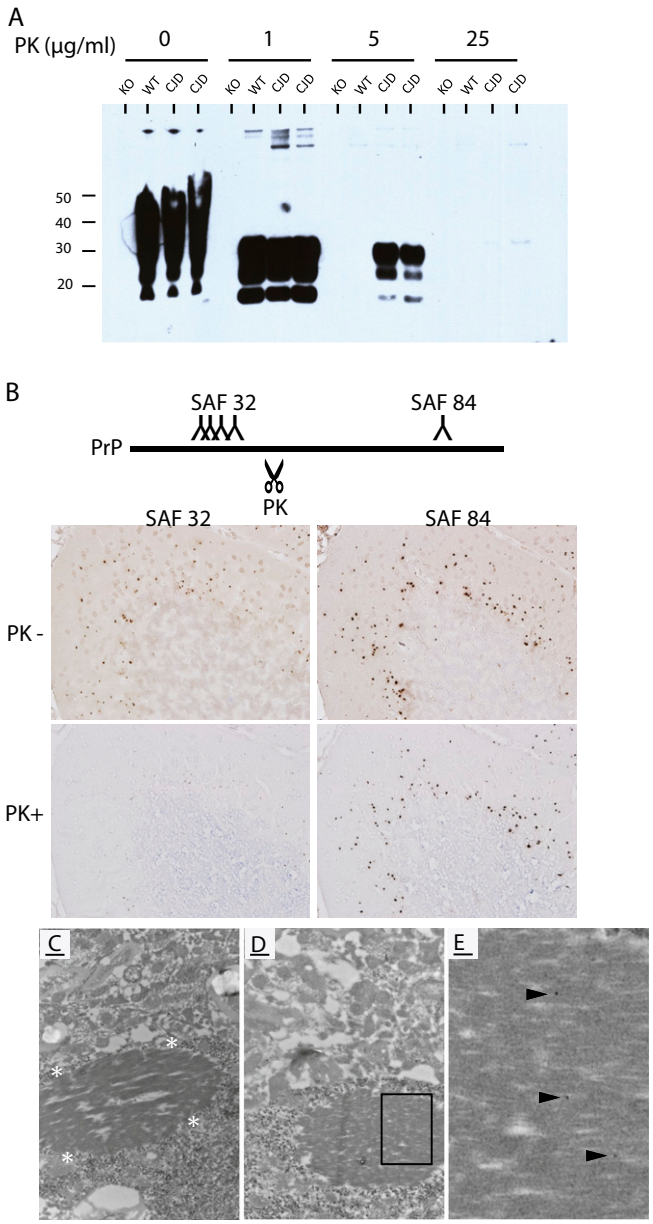

Fig. S5. PrP^{res} and PrP aggregates in FFI and CJD brains. (*A*) Western analysis of cerebellum and brainstem regions digested with PK at various concentrations for 30 min at 37 °C. Low levels of PK (5 μg/mL) yielded truncated PrP fragments in CJD brains, but not in WT brains. However, conventional amounts of PK (25 μg/mL) resulted in nearly complete digestion of PrP in CJD lanes. (*B*) Serial sections of a cerebellar folium were incubated in PBS solution with or without PK (PK+ or PK−), followed by immunostaining for antibodies against the N or C terminus of PrP (SAF32 or SAF84, respectively). Aggregates in CJD mice are composed of PrP that is reactive with SAF32, indicating that PrP containing the N terminus (and likely full length) is aggregating. The N terminus is sensitive to PK, like the PrP^{res} detected in human prion diseases and mouse models of acquired prion diseases. (*C*–*E*) PrP deposits in FFI mice. (*C*) An example of a deposit in a FFI thalamus, revealed by standard EM, is framed by four white asterisks. (*D* and *E*) An example of a deposit in a FFI thalamus, revealed by immuno-EM using mild fixation. (*E*) Higher magnification of the area marked in *D* with the black rectangle. Arrowheads in *E* mark immunogold particles. (Scale bars: *C* and *D*, 500 nm; *E*, 62.5 nm.)

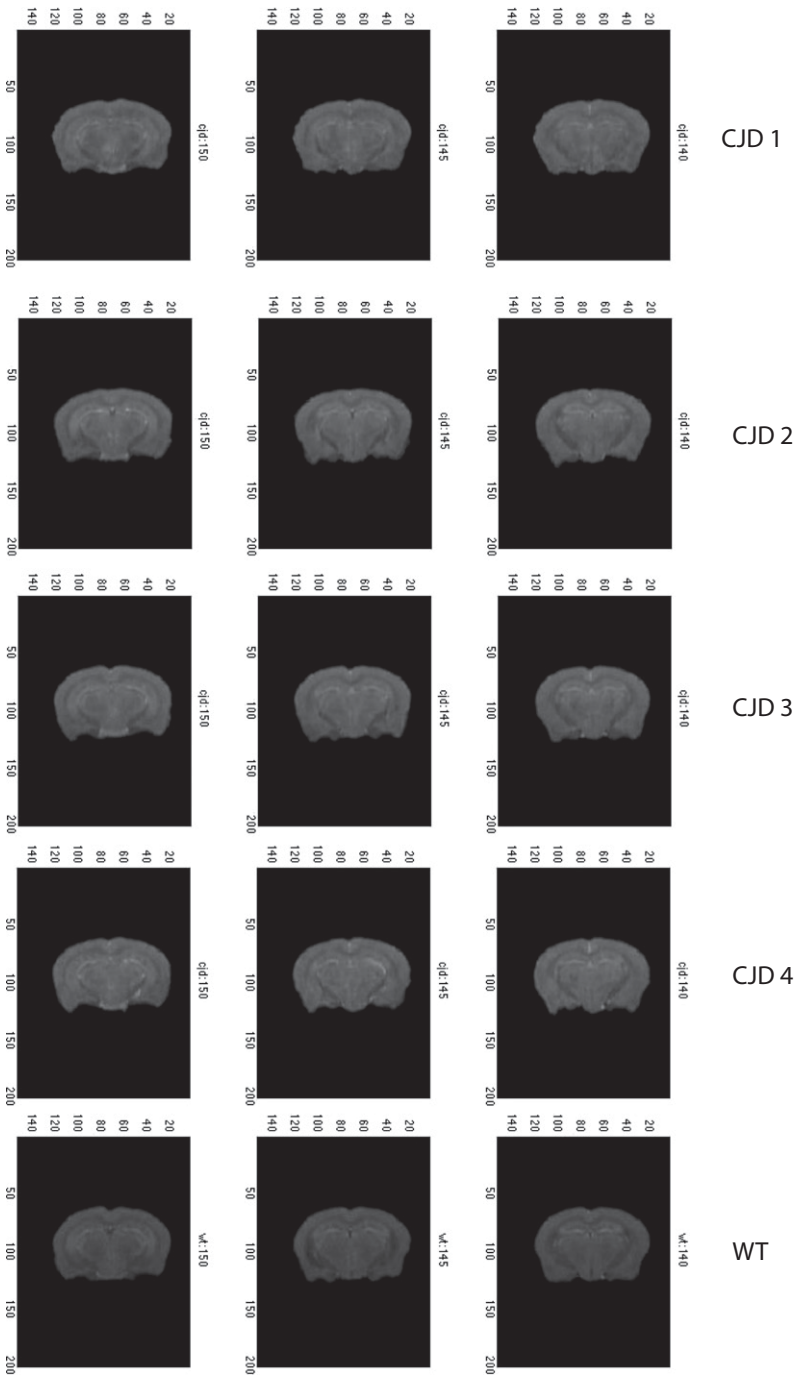

Fig. S6. MRI of CJD mice reveals no gross structural changes compared with control mice. Each column represents slices corresponding to figures in the mouse brain atlas by Paxinos and Franklin (1). An 18-mo-old WT mouse is shown (*Bottom*) along with four different 18-mo-old CJD mice.

1. Paxinos G, Franklin KBJ (2001) *The Mouse Brain in Stereotaxic Coordinates* (Academic, San Diego), 2nd Ed.

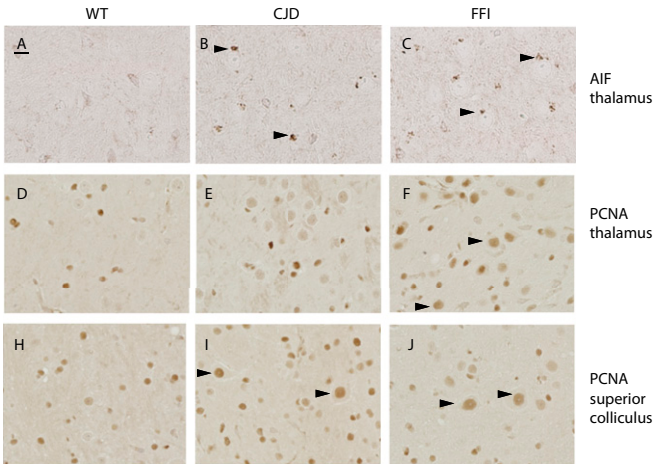

Fig. S7. Activation of cell cycle and death markers. Paraffin-embedded sections from aged WT (*A*, *D*, and *H*), CJD (*B*, *E*, and *I*), and FFI (*C*, *F*, and *J*) mice, stained with antibodies against apoptosis-inducing factor (AIF; *A*–*C*) and PCNA (*D*–*J*). Photographs were taken of the thalamus (*A*–*F*) and superior colliculus (*H*–*J*). Arrowheads in *B* and *C* mark protein staining that is not present in WT brains (*A*). Arrowheads in *E*, *F*, *I*, and *J* mark large, immunopositive neuronal nuclei. Immunopositive nuclei in *D* and *H* are smaller. (Scale bars: *A*–*C*, 0.03 mm; *D*–*J*, 0.05 mm.)

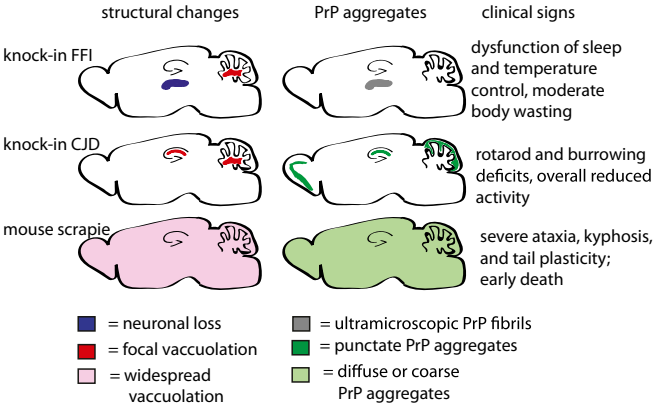

Fig. S8. Selective vulnerability of different prion models. The distribution of structural changes, including neuronal loss and vacuolation, and PrP aggregates are shown for three different mouse models of prion disease. The frequently used models of acquired prion disease, such as scrapie, typically attack the entire brain, whereas the knock-in models of familial prion disease have a more restricted pattern of toxicity, creating an excellent paradigm for the study of selective vulnerability to neurodegenerative disease.

Movie S1. Demonstration of WT mouse in the burrowing apparatus. During actual experiments, a cage lid is in place, the apparatus is in an isolation cubicle, and humans are out of the room.

Movie S1

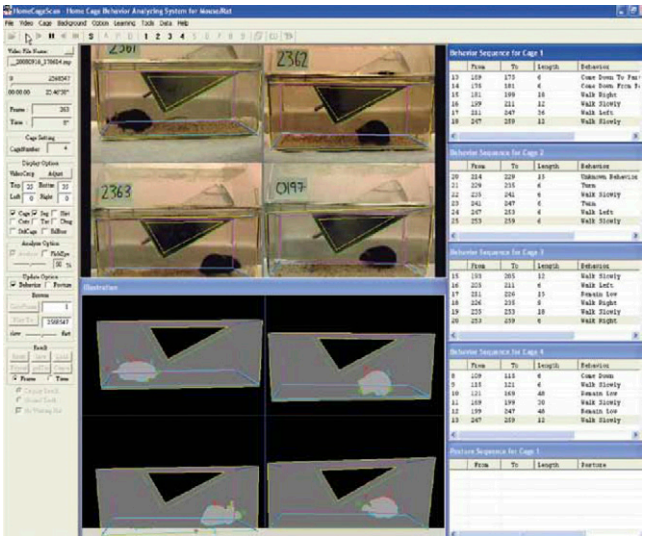

Movie S2. Demonstration of AMBA data being analyzed. (*Upper*) Unprocessed videos of four different cages. (*Lower*) Computed shape and posture of the mouse. Small letters mark regions of the mouse identified by the software. (*Right*) Computed behaviors.

Movie S2

Movie S3. Two Tga20 mice displaying signs of disease caused by injection of CJD mouse brain homogenate.

Movie S3